

# SU(2)-in-SU(1,1) nested interferometer

Wei Du,<sup>1,2</sup> Jia Kong,<sup>3,2</sup> Jun Jia,<sup>1</sup> Sheng Ming,<sup>4</sup> Chun-Hua Yuan,<sup>1</sup>  
J.F.Chen,<sup>5</sup> Z.Y.Ou,<sup>6</sup> Morgan W. Mitchell,<sup>2,7</sup> and Weiping Zhang<sup>4</sup>

<sup>1</sup>Quantum Institute of Light and Atoms, Department of Physics, East China Normal University, Shanghai, 200241, People's Republic of China

<sup>2</sup>ICFO-Institut de Ciències Fotoniques, The Barcelona Institute of Science and Technology, 08860 Castelldefels (Barcelona), Spain

<sup>3</sup>Department of Physics, Hangzhou Dianzi University, Hangzhou 310018, China

<sup>4</sup>Department of Physics and Astronomy, Tsung-Dao Lee Institute, Shanghai Jiao Tong University, Shanghai 200240, People's Republic of China

<sup>5</sup>Shenzhen Institute for Quantum Science and Engineering and Department of Physics, Southern University of Science and Technology, Shenzhen 518055, China

<sup>6</sup>Department of Physics Indiana University-Purdue University Indianapolis, 402 North Blackford Street Indianapolis, Indiana 46202, USA

<sup>7</sup>ICREA – Institució Catalana de Recerca i Estudis Avançats, 08010 Barcelona, Spain

(Dated: June 12, 2025)

The use of squeezing<sup>1,2</sup> and entanglement<sup>3,4</sup> allows advanced interferometers to detect signals that would otherwise be buried in quantum mechanical noise. High sensitivity instruments including magnetometers<sup>5,6</sup> and gravitational wave detectors<sup>7,8</sup> have shown enhanced signal-to-noise ratio (SNR) by injecting single-mode squeezed light into SU(2) interferometers, e.g. the Mach-Zehnder or Michelson topologies. The quantum enhancement in this approach is sensitive to losses, which break the fragile quantum correlations in the squeezed state. In contrast, SU(1,1) interferometers<sup>9</sup> achieve quantum enhancement by noiseless amplification<sup>10</sup>; they noiselessly increase the signal rather than reducing the quantum noise. Prior work on SU(1,1) interferometers has shown quantum enhanced SNR<sup>11</sup> and insensitivity to losses<sup>12,13</sup>, but to date has been limited to low powers and thus low SNR. Here we introduce a new interferometer topology, the SU(2)-in-SU(1,1) nested interferometer, that combines quantum enhancement, the high SNR possible with a SU(2) interferometer, and the loss tolerance of the SU(1,1) approach. We implement this interferometer using four wave mixing in a hot atomic vapor<sup>14</sup>, and demonstrate 2.2(5) dB of quantum SNR enhancement, in a system with a phase variance nearly two orders of magnitude below that of any previous loss-tolerant enhancement scheme<sup>11,12,15</sup>. The new interferometer enables new possibilities such as beyond-shot-noise sensing with wavelengths for which efficient detectors are not available.

The signal-to-noise ratio (SNR) is a central figure of merit in any sensing application. In optical interferometry, the signal strength can be increased by using a larger flux of photons, while quantum noise can be reduced below the shot-noise level using non-classical states of light<sup>1</sup>. Approaches that use single squeezed beams and SU(2) interferometers, e.g. Michelson or Mach-

Zehnder interferometers<sup>16</sup>, have been successful in producing more than 10 dB of noise suppression<sup>17,18</sup>, and have been applied in interferometers with very high photon flux<sup>7,8</sup>, to achieve both large and quantum-enhanced signal-to-noise ratios.

A current limitation of this approach is the loss of squeezing that accompanies optical losses, which break the precise photon-photon correlations of a strongly squeezed state. In Aasi *et al.*<sup>8</sup>, for example, 2.2 dB of extra sensitivity was achieved even though 10.3 dB of squeezing was available, due in large part to the 44% system efficiency.

An alternative approach is to use in-principle-noiseless quantum optical methods to amplify the interferometer signal, rather than aiming to suppress quantum noise. For example, the SU(1,1) interferometer<sup>9</sup> (SUI), illustrated in Fig. 1a, has the topology of the Mach-Zehnder interferometer (MZI), but the splitting and recombination elements are parametric amplifiers (PAs), rather than passive beamsplitters<sup>11</sup>. The SNR of the SUI is insensitive to external loss, i.e., losses outside of the loop formed by the two paths and PAs. In some specific conditions the SUI is also insensitive to internal loss, i.e. losses within this loop<sup>12,13</sup>.

The SUI approach has its own limitations. The PAs, as their name suggests, are used as amplifiers rather than light sources *per se*. To increase photon flux and signal strength, seed light is introduced into the upstream PA to stimulate the generation of bright two-mode squeezed beams. While the PA process can be noiseless in theory, the best implementations to date are based on atomic four-wave mixing (FWM), which inevitably introduces additional noise<sup>19–26</sup>. This FWM noise grows faster with seed power than does the signal, thereby setting an intrinsic limit to SNR. This drawback has to date limited the phase sensing light power to tens of micro-watts in SUI interferometers<sup>11,12,15</sup>.

Here we propose and demonstrate a new SUI-based approach, the SU(2)-in-SU(1,1) nested interferometer (SISNI), which combines advantages of SU(1,1) and

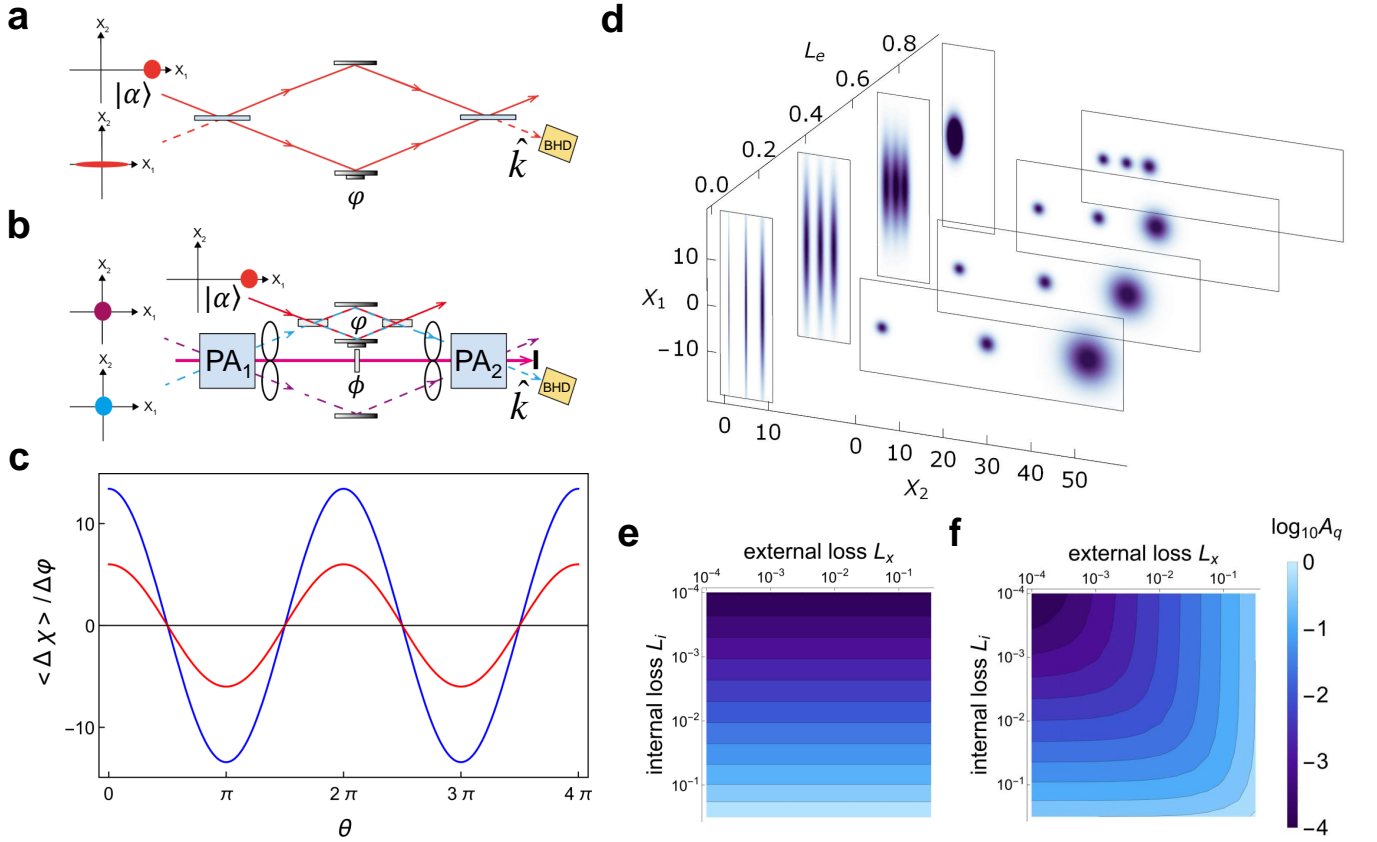


FIG. 1. Comparison of SQ-MZI and SISNI. (a) and (b) show the topology of SQ-MZI and SISNI, respectively. PA: Parametric amplifier; BHD: Balanced homodyne detection. Insets show the various input states in the amplitude quadrature ( $X_1$ ) – phase quadrature ( $X_2$ ) phase space. For both interferometer types, a coherent state  $|\alpha\rangle$  feeds the “bright input” port of the SU(2) interferometer, while a non-classical state feeds the “dark input” port. (c) Signal gain  $d\mathcal{X}/d\varphi$  versus local oscillator phase  $\theta$  for SQ-MZI (red) and SISNI (blue), for the lossless case. Both configurations have  $|\alpha|^2 = 36$  (d) Wigner distributions for the output mode  $\hat{k}$  versus signal phase  $\varphi$  (three equi-spaced values are plotted) and versus external loss  $L_e$ . For larger loss values, degradation of SNR, i.e. overlap of uncertainty areas, is evident in the SQ-MZI case but not that of SISNI. (e) and (f) show the quantum sensitivity advantage  $A_q \equiv \langle \delta\varphi^2 \rangle / \langle \delta\varphi^2 \rangle_{\text{SQL}}$  in dB as a function of internal and external loss for SISNI (left) and SQ-MZI (right).

SU(2) interferometry. As illustrated in Fig. 1b, a SU(2) interferometer is nested inside a SU(1,1) interferometer: the “signal” beam from the upstream PA (PA<sub>1</sub>) is fed into the *dark input* port of a SU(2) interferometer, while a bright coherent state is fed into the *bright input* port. The light emerging from the SU(2) *dark output* port is then recombined with the idler beam in the downstream PA (PA<sub>2</sub>). Our theoretical and experimental results show that this new approach can achieve the large signal strength of SU(2) interferometry and the loss-tolerant quantum noise reduction of the SUI approach.

We note that another modified SUI was recently proposed, the so-called *pumped-up* SUI (puSUI)<sup>27</sup>, which achieves large photon flux by detecting interference of the signal, idler and also pump. This approach appears attractive for atomic interferometry, with possible implementation in spinor BECs or hybrid atom-light systems.

We first calculate the SNR of both squeezed-light-injected MZI (SQ-MZI) and SISNI. In an interferometer

that measures a phase  $\varphi = \varphi_0 + \Delta\varphi$ , where  $\varphi_0$  is the set-point of the interferometer and  $\Delta\varphi$  is the signal, i.e., a small phase excursion to be measured, the SNR  $\zeta$  is defined by

$$\zeta \equiv \frac{\langle \Delta\varphi \rangle^2}{\langle \delta\varphi^2 \rangle} = \frac{\langle \Delta\varphi \rangle^2}{\langle \delta\mathcal{X}^2 \rangle} \left| \frac{\partial \mathcal{X}}{\partial \varphi} \right|^2 = \frac{\langle \Delta\mathcal{X} \rangle^2}{\langle \delta\mathcal{X}^2 \rangle} \quad (1)$$

where  $\langle \delta\varphi^2 \rangle$  is the variance of the phase readout,  $\mathcal{X}$  is the measured observable with variance  $\langle \delta\mathcal{X}^2 \rangle$ , all evaluated at  $\varphi = \varphi_0$ . The signal referred to the output is  $\langle \Delta\mathcal{X} \rangle = \langle \mathcal{X}(\varphi_0 + \Delta\varphi) \rangle - \langle \mathcal{X}(\varphi_0) \rangle$ . The quantum optical performance of each strategy can be analyzed by considering cascaded linear input-output relations (see Methods). In each case, we set  $\varphi_0 = n\pi, n \in \mathbb{Z}$  to work at the dark fringe condition. At the dark fringe, the quantum noise exiting the dark port originates entirely in the quantum state injected to the dark input port. For the SQ-MZI, the dark output port ( $\hat{k}$ ) outputs the injected squeezed state after any internal losses. For SISNI, two

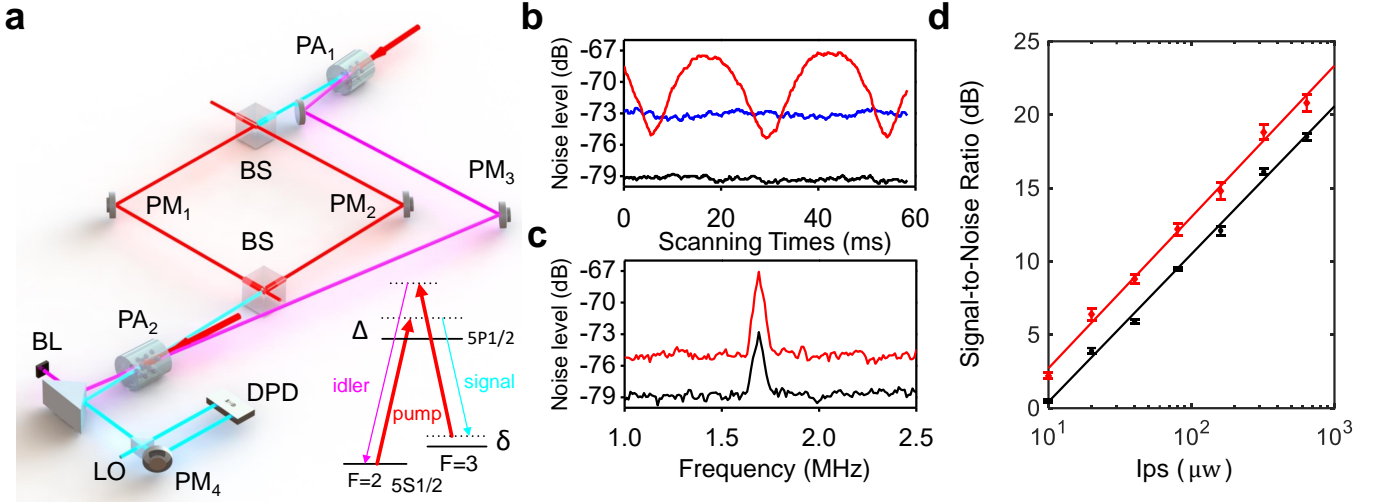


FIG. 2. **Experimental demonstration of quantum enhancement of the SISNI.** (a) Schematic of experiment. PA: Parametric amplifier; BS: 50/50 Beamsplitter; PM: Mirror mounted with piezo-electric transducer as phase modulator; LO: Local oscillator; DPD: Differential photodetector; BL: Beam block. Inset shows the double- $\Lambda$  level structure of the PA process, which uses the D1 line of  $^{85}\text{Rb}$ . The two pump beams (red arrows) are frequency degenerate,  $\Delta = 1$  GHz and  $\delta = 2$  MHz. PA<sub>1</sub> and PA<sub>2</sub> act as a source of two-mode squeezing and amplifier, respectively. (b) Noise of the MZI and SISNI. Graph shows measured noise of the output phase quadrature in a bandwidth of 100 kHz about 1.7 MHz, versus time as  $\phi$ , the relative phase of the PAs, is scanned using PM<sub>3</sub>. MZI phase is locked to dark fringe. Traces show: MZI SQL (black), implemented by blocking both PA pumps, MZI output amplified by PA<sub>2</sub> (blue), implemented by blocking only PA<sub>1</sub> pump, and SISNI. (c) Measured noise spectra of MZI (black) and SISNI (red) outputs, acquired as in (b), but with PAs relative phase locked to noise minimum and a sinusoidal phase signal at 1.7 MHz applied via PM<sub>1</sub>. (d) Measured SNR, defined as spectral peak over white background level from spectra as in (c), versus coherent state power  $|\alpha|^2$  for MZI (black) and SISNI (red). Error bars show  $\pm 1\sigma$  statistical variation. Lines show fits with  $\text{SNR} = A|\alpha|^2$ .

output ports are both dark, however the output signal at mode  $\hat{k}$  is slightly stronger than at  $\hat{j}$ . For this reason, it is sufficient to perform a balanced homodyne detection on output  $\hat{k}$ , i.e., to measure  $\mathcal{X} = X_{\hat{k}}(\theta) \equiv e^{-i\theta}\hat{k} + e^{i\theta}\hat{k}^\dagger$ , as shown in Fig. 1 a and b.  $\theta$  is the relative phase between local oscillator and  $\hat{k}$ . Fig. 1 c shows the output signal slope  $\langle \Delta \mathcal{X} \rangle / \Delta \varphi$  versus  $\theta$  (not considering losses), showing that  $\theta = n\pi$  gives the largest signal slope  $d\mathcal{X}/d\varphi$ . From here forward we take  $\mathcal{X} = i(\hat{k}^\dagger - \hat{k}) \equiv X_2$ . To simultaneously minimize  $\langle \delta \mathcal{X}^2 \rangle$  in the SQ-MZI, we assume  $X_2$ -squeezed vacuum is injected into the dark input port.

At these optimal conditions, we calculate the SNR of both SQ-MZI and SISNI output observables including the effects of loss (see Methods). For the SQ-MZI, the optimized SNR is

$$\zeta_{\text{SQ-MZI}} = \frac{\eta(\Delta\varphi)^2|\alpha|^2}{\eta(G+g)^{-2} + L_i(1-L_e) + L_e}, \quad (2)$$

where  $\eta = (1-L_i)(1-L_e)$ , and  $L_i$  and  $L_e$  are internal and external loss for the interferometer respectively.  $|\alpha|^2$  is the input power and  $(G+g)^{-2}$  indicates the degree of squeezing of the dark port input. When  $(G+g)^{-2} = 1$ , the above equation describes a conventional MZI with SQL sensitivity. For the SISNI, the optimized SNR is

$$\zeta_{\text{SISNI}} = \frac{\eta_s G_2^2 (\Delta\varphi)^2 |\alpha|^2}{L + (\eta_s G_1 G_2 - \eta_i g_1 g_2)^2 + (\eta_s g_1 G_2 - \eta_i G_1 g_2)^2}, \quad (3)$$

where  $\eta_s = (1-L_{is})(1-L_e)$ ,  $\eta_i = (1-L_{ii})(1-L_e)$ ,  $L = L_e + g_2^2(1-L_e)L_{ii} + G_2^2(1-L_e)L_{is}$ , and  $L_\beta$  with  $\beta \in \{is, ii, e\}$  indicates internal loss of the signal mode (including loss in the SU(2) interferometer) and idler mode of the SU(1,1) interferometer, and external loss after PA<sub>2</sub>.  $G_1 = \sqrt{1+g_1^2}$  and  $G_2 = \sqrt{1+g_2^2}$  are the amplification gains of PA<sub>1</sub> and PA<sub>2</sub>, respectively, where  $1/(G_1+g_1)^2$  indicates the degree of two-mode squeezing generated by PA<sub>1</sub>. Eq. (3) shows the same noise performance as the SUI, which improves the SNR relative to the conventional MZI with the same  $|\alpha|^2$ , while also allowing operation at large  $|\alpha|^2$ .

To demonstrate the above-described quantum advantage at large signal strength, we implemented a SISNI as shown in Fig. 2a. PA<sub>1</sub> and PA<sub>2</sub> are implemented as FWM processes<sup>28</sup> in  $^{85}\text{Rb}$ , with amplification gains  $G_1$  and  $G_2$ . A MZI, formed by two linear beam splitters and mirrors with piezoelectric transducers (PZTs) is nested in one arm of the SUI. The two input ports of PA<sub>1</sub> are fed with vacuum, to minimize FWM noise. Laser light is injected into the bright input port of the MZI. Local oscillator (LO) beams are generated by FWM process to implement balanced homodyne detection (BHD). We note that the interferometer becomes a simple MZI if the PAs' pump light is blocked. The relative phase  $\phi$  of the two PA pumps is locked to minimum net amplification by a quantum noise locking technique<sup>29</sup>, and a coherent modulated locking technique is used to maintain the MZI

at the dark fringe condition<sup>30,31</sup>. To lock the phase of the LO on the phase quadrature, we use a method described by Liu et al.<sup>32</sup>, in which the input coherent state is amplitude modulated and the envelope of modulations seen at the HD is fed back to the LO phase.

The output performance of SISNI and MZI under the same operating conditions are shown in Fig. 2. The black trace is the output noise level of MZI at the dark fringe, which is also the vacuum noise level. The blue trace shows the noise level of PA<sub>2</sub>. We define the ratio of PA output noise to vacuum noise, here 6 dB, as the quantum noise gain (QNG)  $G_q$ , which for an ideal PA is  $G_q = G^2 + g^2$ . The red trace presents noise reduction (minimum) and anti-reduction (maximum) by scanning the phase of twin beams with the MZI locked at the dark fringe. It shows 2.4 dB of noise reduction below the noise level of PA<sub>2</sub>, while the QNG of PA<sub>1</sub> is set as 4 dB. The inset shows the power spectrum of MZI (Black trace) and SISNI (Red trace) when a signal at 1.7 MHz is introduced by modulating the PZT. As above, both the MZI and SUI are locked at their respective dark conditions. The SNR<sup>33</sup> of the MZI and SISNI are 4.8(2) dB and 7.0(3) dB, respectively, which indicates a 2.2(5) dB SNR enhancement. This is the best SNR enhancement we could achieve by optimizing the QNG. The limitation is mainly due to losses coming from optical mirrors, atomic absorption and dephasing noise. For example, the total internal losses caused by mirrors at signal and idler arms are 16% and 10% respectively. Considering all these loss effects, we build a more complete theory which predicts well our experimental optimizing process (see Methods).

To verify that our scheme is able to maintain the SNR enhancement at high photon flux, we measure the SNR of MZI and SISNI while increasing the laser input power. As can be seen in Fig. 2d, both MZI and SISNI performance are well fit by  $\text{SNR} = A|\alpha|^2$ , which confirms their photon shot noise limited performance. By the fit, the SISNI SNR is 2.2 dB above that of the MZI, and is observed up to nearly 1 mW, which is hundreds of times higher than the  $\mu\text{W}$  levels of previous SUIs<sup>11,12,15,34</sup>.

The SISNI is tolerant of loss in the detection process, because the PA process boosts the signal above the vacuum noise level. PA processes, e.g. FWM, have

been demonstrated from radio<sup>35</sup> to XUV<sup>36</sup> wavelengths, whereas high quantum-efficiency detectors exist for a much more limited range. The SISNI thus makes possible sensitive, quantum-enhanced measurements in previously inaccessible spectral regions.

In conclusion, we have demonstrated a new interferometer topology, the SU(2)-in-SU(1,1) nested interferometer. A detailed analysis shows that this topology combines the loss-tolerance of SU(1,1) interferometry with the large signal strength of SU(2) interferometry. Experimentally, we have demonstrated 2.2 dB of signal-to-noise ratio improvement beyond the standard quantum limit, with optical power levels, and thus signal-to-noise ratios, beyond the reach of traditional SU(1,1) interferometry. The new interferometer has features very appealing for extreme sensing with optical interferometers.

### Acknowledgments

W.D. acknowledges support by study abroad program East China Normal University. W.Z. acknowledge support by the National Key Research and Development Program of China under Grant number 2016YFA0302001, and the National Natural Science Foundation of China (NSFC) through Grant No. 11654005, Science and Technology Commission of Shanghai Municipality (STCSM) (16DZ2260200). J. K. acknowledges the support from NSFC through Grant No. 11935012. J.F.C. acknowledge the support from NSFC through Grant No. 11674100 and Shanghai Rising-Star Program No. 17QA1401300. C.H.Y. acknowledge the support from NSFC through Grant No. 11974111 and No. 11474095. M. W. M. acknowledges Spanish MINECO projects OCARINA (Grant Ref. PGC2018-097056-B-I00) and Q-CLOCKS (PCI2018-092973), the Severo Ochoa programme (SEV-2015-0522); Agència de Gestió d'Ajuts Universitaris i de Recerca (AGAUR) project (2017-SGR-1354); Fundació Privada Cellex and Generalitat de Catalunya (CERCA program, RIS3CAT project QuantumCAT); Quantum Technology Flagship projects MACQSIMAL (820393) and QRANGE (820405); Marie Skłodowska-Curie ITN ZULF-NMR (766402); 17FUN03-USOQS, which has received funding from the EMPIR programme co-financed by the Participating States and from the European Union's Horizon 2020 research and innovation programme.

<sup>1</sup> C. M. Caves, Phys. Rev. D **23**, 1693 (1981).

<sup>2</sup> R. E. Slusher, L. W. Hollberg, B. Yurke, J. C. Mertz, and J. F. Valley, Physical Review Letters **55**, 2409 (1985).

<sup>3</sup> M. J. Holland and K. Burnett, Physical Review Letters **71**, 1355 (1993).

<sup>4</sup> M. W. Mitchell, J. S. Lundeen, and A. M. Steinberg, Nature **429**, 161 (2004).

<sup>5</sup> F. Wolfgramm, A. Cerè, F. A. Beduini, A. Predojević, M. Koschorreck, and M. W. Mitchell, Physical Review Letters **105**, 053601 (2010).

<sup>6</sup> T. Horrom, R. Singh, J. P. Dowling, and E. E. Mikhailov,

Phys. Rev. A **86**, 023803 (2012).

<sup>7</sup> The LIGO Scientific Collaboration, Nat Phys **7**, 962 (2011).

<sup>8</sup> J. Aasi, et al., Nat Photon **7**, 613 (2013).

<sup>9</sup> B. Yurke, S. L. McCall, and J. R. Klauder, Phys. Rev. A **33**, 4033 (1986).

<sup>10</sup> C. M. Caves, Phys. Rev. D **26**, 1817 (1982).

<sup>11</sup> F. Hudelist, J. Kong, C. Liu, J. Jing, Z. Y. Ou, and W. Zhang, Nature Communications **5**, 3049 (2014).

<sup>12</sup> M. Manceau, G. Leuchs, F. Khalili, and M. Chekhova, Phys. Rev. Lett. **119**, 223604 (2017).

- <sup>13</sup> J. Xin, H. Wang, and J. Jing, *Applied Physics Letters* **109**, 051107 (2016).
- <sup>14</sup> C. F. McCormick, V. Boyer, E. Arimondo, and P. D. Lett, *Optics Letters*, *Optics Letters* **32**, 178 (2007).
- <sup>15</sup> D. Linnemann, H. Strobel, W. Muessel, J. Schulz, R. J. Lewis-Swan, K. V. Kheruntsyan, and M. K. Oberthaler, *Phys. Rev. Lett.* **117**, 013001 (2016).
- <sup>16</sup> B. Yurke, S. L. McCall, and J. R. Klauder, *Phys. Rev. A* **33**, 4033 (1986).
- <sup>17</sup> M. Mehmet, S. Ast, T. Eberle, S. Steinlechner, H. Vahlbruch, and R. Schnabel, *Opt. Express* **19**, 25763 (2011).
- <sup>18</sup> H. Vahlbruch, M. Mehmet, K. Danzmann, and R. Schnabel, *Phys. Rev. Lett.* **117**, 110801 (2016).
- <sup>19</sup> A. L. Gaeta, R. W. Boyd, and G. S. Agarwal, *Phys. Rev. A* **46**, 4271 (1992).
- <sup>20</sup> R. W. Schirmer, M. Y. Lanzerotti, A. L. Gaeta, and G. S. Agarwal, *Phys. Rev. A* **55**, 3155 (1997).
- <sup>21</sup> R. Boyd, G. Agarwal, W. Davis, A. Gaeta, E. Nagasako, and M. Kauranen, *Acta Physica Polonica A* **86**, 117 (1994).
- <sup>22</sup> M. Kauranen, A. L. Gaeta, and R. W. Boyd, *Optics communications* **103**, 211 (1993).
- <sup>23</sup> V. V. Iruvanti and R. W. Boyd, *Optics communications* **118**, 46 (1995).
- <sup>24</sup> W. V. Davis, M. Kauranen, E. M. Nagasako, R. J. Gehr, A. L. Gaeta, R. W. Boyd, and G. S. Agarwal, *Phys. Rev. A* **51**, 4152 (1995).
- <sup>25</sup> M. T. L. Hsu, G. Hétet, A. Peng, C. C. Harb, H.-A. Bachor, M. T. Johnsson, J. J. Hope, P. K. Lam, A. Dantan, J. Cviklinski, A. Bramati, and M. Pinard, *Phys. Rev. A* **73**, 023806 (2006).
- <sup>26</sup> M. Kauranen, A. L. Gaeta, R. W. Boyd, and G. S. Agarwal, *Phys. Rev. A* **50**, R929 (1994).
- <sup>27</sup> S. S. Szigeti, R. J. Lewis-Swan, and S. A. Haine, *Phys. Rev. Lett.* **118**, 150401 (2017).
- <sup>28</sup> C. F. McCormick, A. M. Marino, V. Boyer, and P. D. Lett, *Phys. Rev. A* **78**, 043816 (2008).
- <sup>29</sup> K. McKenzie, E. E. Mikhailov, K. Goda, P. K. Lam, N. Grosse, M. B. Gray, N. Mavalvala, and D. E. McClelland, *Journal of Optics B: Quantum and Semiclassical Optics* **7**, S421 (2005).
- <sup>30</sup> H. Wang, A. M. Marino, and J. Jing, *Applied Physics Letters* **107**, 121106 (2015).
- <sup>31</sup> W. Du, J. Jia, J. F. Chen, Z. Y. Ou, and W. Zhang, *Opt. Lett.* **43**, 1051 (2018).
- <sup>32</sup> Y. Liu, J. Li, L. Cui, N. Huo, S. M. Assad, X. Li, and Z. Y. Ou, *Opt. Express* **26**, 27705 (2018).
- <sup>33</sup> J. Kong, F. Hudelist, Z. Y. Ou, and W. Zhang, *Phys. Rev. Lett.* **111**, 033608 (2013).
- <sup>34</sup> S. Liu, Y. Lou, J. Xin, and J. Jing, *Phys. Rev. Applied* **10**, 064046 (2018).
- <sup>35</sup> J. F. Federici, *IEEE Transactions on Plasma Science*, *IEEE Transactions on Plasma Science* **19**, 549 (1991).
- <sup>36</sup> F. Bencivenga, R. Cucini, F. Capotondi, A. Battistoni, R. Mincigrucci, E. Giangrisostomi, A. Gessini, M. Manfreda, I. P. Nikolov, E. Pedersoli, E. Principi, C. Svetina, P. Parisse, F. Casolari, M. B. Danailov, M. Kiskinova, and C. Masciovecchio, *Nature* **520**, 205 (2015).
- <sup>37</sup> Z. Y. Ou, *Phys. Rev. A* **85**, 023815 (2012).

## Methods

**Input-output relations.** The topology of the SQ-MZI and SISNI are shown in Figs. 3 and 4, respectively. Labels indicate modes at the corresponding positions. To avoid confusion with the SISNI discussion that follows, we label MZI modes with the subscript <sub>M</sub>. Each interferometer operation can be described by a sequence of linear transformations. For the SQ-MZI, these are

$$\hat{b}_M = G\hat{a}_M + g\hat{a}_M^\dagger \quad (4)$$

$$\hat{c}_M = \sqrt{1-L_i}(\sqrt{T}\hat{b}_M + \sqrt{R}\hat{A}_M) + \sqrt{L_i}\hat{B}_M \quad (5)$$

$$\hat{d}_M = e^{i\varphi}\sqrt{1-L_i}(\sqrt{T}\hat{A}_M - \sqrt{R}\hat{b}_M) + \sqrt{L_i}\hat{C}_M \quad (6)$$

$$\hat{e}_M = \sqrt{T}\hat{c}_M + \sqrt{R}\hat{d}_M \quad (7)$$

$$\hat{k}_M = \sqrt{1-L_e}\hat{g}_M + \sqrt{L_e}\hat{D}_M. \quad (8)$$

Here  $G = \sqrt{1+g^2}$  is the amplification gain,  $L_i$  and  $L_e$  indicate internal and external losses, respectively.  $\hat{B}_M, \hat{C}_M$  and  $\hat{D}_M$  describe vacuum modes introduced by the loss processes. Because  $g$  and  $G$  are real, the phase quadrature is squeezed by the PA. The input mode is vacuum for mode  $\hat{a}$  and a coherent state  $|\alpha\rangle$  for  $\hat{A}_M$ . For  $T = R = 1/2$ , the case of interest, this simplifies to

$$\hat{k}_M = \hat{N}_M + \sqrt{\eta}[\tilde{S}\hat{A}_M - \tilde{C}(G\hat{a}_M + g\hat{a}_M^\dagger)], \quad (9)$$

where  $\hat{N}_M = \sqrt{L_e}\hat{D}_M + (\sqrt{L_i(1-L_e)}/2\hat{B}_M + \sqrt{L_i(1-L_e)}/2\hat{C}_M)$ ,  $\eta = (1-L_i)(1-L_e)$ ,  $\tilde{S} = (e^{i\varphi} + 1)/2$  and  $\tilde{C} = (e^{i\varphi} - 1)/2$ .

The signal is given by the phase quadrature  $\mathcal{X} = X_{2,M} \equiv i(\hat{k}_M^\dagger - \hat{k}_M)$ . Near the dark fringe condition,  $\varphi = \pi + \Delta\varphi$ ,  $\Delta\varphi \ll \pi$ , the mean signal evaluates to

$$\langle \Delta\mathcal{X} \rangle = \langle \Delta X_{2,M} \rangle = -\sqrt{\eta}\Delta\varphi|\alpha|. \quad (10)$$

At this same condition the noise variance is

$$\begin{aligned} \langle \Delta\mathcal{X}^2 \rangle &= \langle \delta^2 X_{2,M} \rangle \\ &= \langle X_{2,M}^2 \rangle - \langle X_{2,M} \rangle^2 \\ &= \eta \left( \frac{1 + \cos\varphi}{2} + \frac{1}{(G+g)^2} \frac{1 - \cos\varphi}{2} \right) + L_i(1-L_e) + L_e \end{aligned} \quad (11)$$

$$= \frac{\eta}{(G+g)^2} + L_i(1-L_e) + L_e \quad (12)$$

Then we find the SNR

$$\zeta_{\text{SQ-MZI}} = \frac{\eta(\Delta\varphi)^2|\alpha|^2}{\eta(G+g)^{-2} + L_i(1-L_e) + L_e}. \quad (13)$$

and phase variance

$$\langle \Delta\varphi^2 \rangle = \frac{\eta(G+g)^{-2} + L_i(1-L_e) + L_e}{\eta|\alpha|^2}, \quad (14)$$

For the SISNI the linear transformations are

$$\hat{c} = G_1\hat{b} + g_1\hat{a}^\dagger \quad (15)$$

$$\hat{d} = G_1\hat{a} + g_1\hat{b}^\dagger \quad (16)$$

$$\hat{e} = e^{i\phi}\sqrt{1-L_{ii}}\hat{c} + \sqrt{L_{ii}}\hat{B} \quad (17)$$

$$\hat{G} = \sqrt{1-L_{is}}(\sqrt{T}\hat{d} + \sqrt{R}\hat{A}) + \sqrt{L_{is}}\hat{D} \quad (18)$$

$$\hat{H} = e^{i\varphi}\sqrt{1-L_{is}}(\sqrt{T}\hat{A} - \sqrt{R}\hat{d}) + \sqrt{L_{is}}\hat{C} \quad (19)$$

$$\hat{f} = \sqrt{T}\hat{G} + \sqrt{R}\hat{H} \quad (20)$$

$$\hat{g} = G_2\hat{f} + g_2\hat{e}^\dagger \quad (21)$$

$$\hat{h} = G_2\hat{e} + g_2\hat{f}^\dagger \quad (22)$$

$$\hat{k} = \sqrt{1-L_e}\hat{g} + \sqrt{L_e}\hat{E} \quad (23)$$

$$\hat{j} = \sqrt{1-L_e}\hat{h} + \sqrt{L_e}\hat{F}, \quad (24)$$

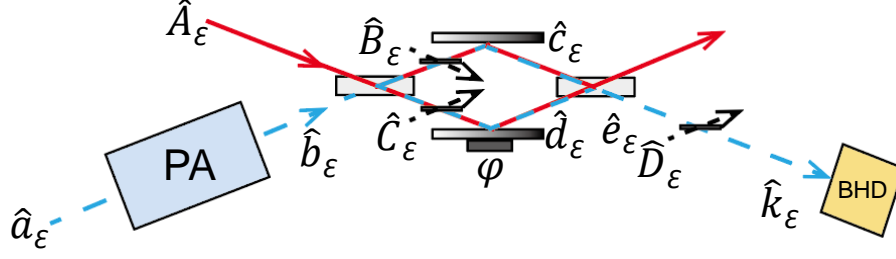


FIG. 3. Squeezed light injected MZI.

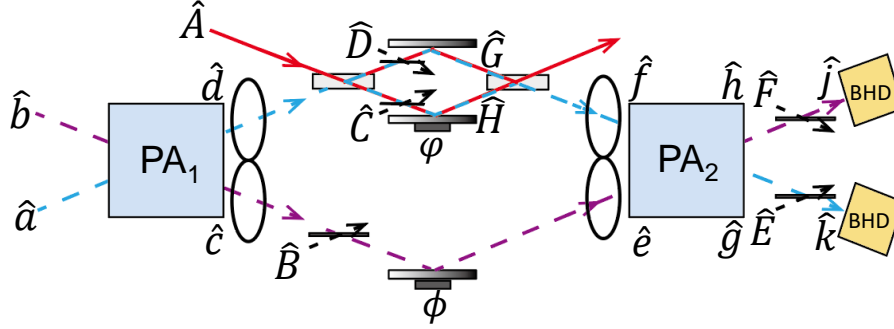


FIG. 4. SU2-in-SU(1,1) nested interferometer.

where  $G_1 = \sqrt{1 + g_1^2}$  and  $G_2 = \sqrt{1 + g_2^2}$  are the amplification gains of PA<sub>1</sub> and PA<sub>2</sub>,  $L_\beta$  with  $\beta \in \{is, ii, e\}$  indicates internal loss at signal mode ( $\hat{d}$ ) and idler mode ( $\hat{c}$ ) and external loss after PA<sub>2</sub>.  $\hat{B}, \hat{C}, \hat{D}, \hat{E}$  and  $\hat{F}$  are vacuum modes introduced by the loss channels.

The output mode  $\hat{k}$  can be expressed as:

$$\hat{k} = \hat{N}_i + \sqrt{\eta_s}[G_2(\tilde{S}\hat{A} - \tilde{C}(G_1\hat{a} + g_1\hat{b}^\dagger))] + e^{-i\phi}\sqrt{\eta_i}g_2(G_1\hat{b}^\dagger + g_1\hat{a}), \quad (25)$$

where  $\hat{N}_i = \sqrt{L_e}\hat{E} + g_2\sqrt{L_{ii}(1-L_e)}\hat{B} + G_2(\sqrt{L_{is}(1-L_e)}/2\hat{C} + \sqrt{L_{ii}(1-L_e)}/2\hat{D})$ ,  $\eta_s = (1-L_{is})(1-L_e)$ ,  $\eta_i = (1-L_{ii})(1-L_e)$ , and  $\phi$  is the relative phase between two PAs.

We assume  $\phi = \pi$ , i.e. the SUI locked to minimum net amplification, consider again the dark fringe condition  $\varphi = \pi + \Delta\varphi$ ,  $\Delta\varphi \ll \pi$ , and evaluate the signal and noise of  $\mathcal{X} = X_2 \equiv i(\hat{k}^\dagger - \hat{k})$ . The mean signal is

$$\langle \Delta\mathcal{X} \rangle = \langle \Delta X_2 \rangle = -\sqrt{\eta_s}G_2\Delta\varphi|\alpha|, \quad (26)$$

and variance is

$$\begin{aligned} \langle \delta^2 X_2 \rangle &= \langle X_2^2 \rangle - \langle X_2 \rangle^2 \\ &= L + \eta_s[G_2^2 \frac{1 + \cos \varphi}{2} + G_2^2(G_1^2 + g_1^2) \frac{1 - \cos \varphi}{2}] + \eta_i g_2^2(G_1^2 + g_1^2) - 2\sqrt{\eta_s \eta_i} G_1 G_2 g_1 g_2 (\cos \varphi - 1) \cos \phi \end{aligned} \quad (27)$$

$$= L + (\sqrt{\eta_s}G_1G_2 - \sqrt{\eta_i}g_1g_2)^2 + (\sqrt{\eta_s}g_1G_2 - \sqrt{\eta_i}G_1g_2)^2 \quad (28)$$

where  $L = L_e + g_2^2(1-L_e)L_{ii} + G_2^2(1-L_e)L_{is}$ . The SNR is

$$\zeta_{\text{SISNI}} = \frac{\langle \Delta X_2 \rangle^2}{\langle \delta^2 X_2 \rangle} = \frac{\eta_s G_2^2 (\Delta\varphi)^2 |\alpha|^2}{L + (\sqrt{\eta_s}G_1G_2 - \sqrt{\eta_i}g_1g_2)^2 + (\sqrt{\eta_s}g_1G_2 - \sqrt{\eta_i}G_1g_2)^2} \quad (29)$$

and the phase variance is

$$\langle \Delta\varphi^2 \rangle = \frac{L + (\sqrt{\eta_s}G_1G_2 - \sqrt{\eta_i}g_1g_2)^2 + (\sqrt{\eta_s}g_1G_2 - \sqrt{\eta_i}G_1g_2)^2}{\eta_s G_2^2 |\alpha|^2}. \quad (30)$$

In the simplest case of no loss and  $G_1 = G_2$ , the SNR and phase variance reduce to

$$\zeta_{\text{SISNI}} = G_2^2 (\Delta\varphi)^2 \alpha^2 \quad (31)$$

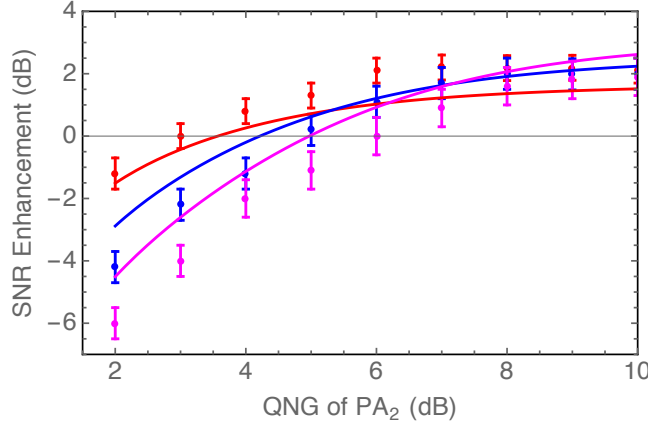


FIG. 5. **Characterization of the trade-off between gain and FWM noise in the SISNI.** Horizontal axis shows quantum noise gain (QNG),  $G_{q2} \equiv G_2^2 + g_2^2$ , adjusted by control of the power of pump light. Vertical axis shows the SNR enhancement of the SISNI over the MZI at equal coherent state input power, with positive values indicating advantage for the SISNI. Points and error bars indicate mean and plus/minus one standard deviation from repeated measurements. Red, blue and magenta data points and curves correspond to  $PA_1$  QNG levels 4 dB, 6 dB and 8 dB, respectively. Curves show fits based on PA noise model, see Section “Parametric amplifier noise model.”

and

$$\langle \Delta \varphi^2 \rangle = \frac{1}{G_2^2 |\alpha|^2}, \quad (32)$$

respectively.

**Optimization of parametric amplifier gain factors.** Our two-mode squeezed light is generated through a FWM process in hot atomic vapor. In this process, higher optical depth (OD) increases the gain, but also introduces excess noise due to atomic dephasing, which is a key factor limiting squeezing generation. The second FWM process ( $PA_2$ ) adds extra noise through this same mechanism. In the SISNI and SUI schemes, the cascaded PA process is still more sensitive to atomic dephasing because the excess noise generated in  $PA_1$  is amplified when it reaches  $PA_2$ , a stimulated FWM process. To understand the tradeoff between OD and dephasing, we studied the SNR enhancement of SISNI relative to the MZI for different values of the quantum noise gain (QNG)  $G_{q\text{meas}} = \langle \delta^2 \hat{X}_{\text{meas}}(\theta) \rangle$  when the inputs to the amplifier are vacuum and where  $m \in \{1, 2\}$  indicates  $PA_m$ . Results shown in Fig. 5. As seen there, the SNR enhancement increases with increasing  $QNG_2$  until saturation, but (at least in the range studied) decreases with increasing  $QNG_1$ . Based on these results we chose  $G_{q1} = 4$  dB and  $G_{q2} = 6$  dB as the conditions for the experiments described in the main text.

**Parametric amplifier noise model.** To understand the gain-advantage relationship described in the previous section and seen in Figure 5, we must modify the noise model of the PAs, which until this point have been described as ideal two-mode squeezers. An accurate and detailed model of noise in FWM processes is beyond the scope of this manuscript, but we can obtain qualitative insights by adapting a simple physical model described previously<sup>37</sup>. In this model,  $PA_1$  has the input-output relations

$$\hat{c} = \bar{G}_1 \hat{b} + \bar{g}_1 \hat{a}^\dagger + \bar{G}'_1 \hat{b}_0 + \bar{g}'_1 \hat{a}_0^\dagger \quad (33)$$

$$\hat{d} = \bar{G}_1 \hat{a} + \bar{g}_1 \hat{b}^\dagger + \bar{G}'_1 \hat{a}_0 + \bar{g}'_1 \hat{b}_0^\dagger, \quad (34)$$

where  $\hat{a}_0$  and  $\hat{b}_0$  are auxiliary modes. Here we take these to be in thermal states with quadrature variances  $\langle \Delta X^2 \rangle = \langle \Delta P^2 \rangle \equiv \epsilon^2 \geq 1$ . The input-output relations for  $PA_2$  are the same as above with the substitutions  $\hat{a} \rightarrow \hat{e}$ ,  $\hat{b} \rightarrow \hat{f}$ ,  $\hat{c} \rightarrow \hat{g}$ ,  $\hat{d} \rightarrow \hat{h}$ , and  $1 \rightarrow 2$ . The coupling factors are (subscripts  $i = 1, 2$  indicating which PA are henceforth omitted):  $\bar{G} = [(1 - \rho^2)/4 + |\kappa|^2]/M$ ,  $\bar{g} = \kappa/M$ ,  $\bar{G}' = \sqrt{\rho}(1 + \rho)/(2M)$  and  $\bar{g}' = \kappa\sqrt{\rho}/M$ , where  $M = (1 + \rho)^2/4 - |\kappa|^2$ . Loss and gain are parametrized by  $\rho$  and  $\kappa$ , respectively. This model originates in the description of lossy, cavity-based two-mode parametric amplifiers, and for this reason is not expected to match quantitatively the single-pass FWM we use here. Nonetheless, it has qualitative features appropriate to the FWM scenario, e.g. the noise introduced by loss is amplified by the gain process. We note that for given  $\epsilon^2$  and  $\rho, \kappa$  can be found from the QNG.



To compare against the measured SNR enhancement, we use the measured loss values  $L_{is} = 0.16$ ,  $L_{ii} = 0.1$ ,  $L_e = 0.15$ , and the above input-output relations in place of Eqs. (15),(16) for PA<sub>1</sub> and Eqs. (21), (21) for PA<sub>2</sub>. By the same mathematical machinery described above we compute  $\zeta_{\text{SISNI}}$  and the SNR advantage relative to the SQL. Fitting to the measured data we find best fit parameters  $\rho_1/\gamma_1 = 5 \times 10^{-4}$ ,  $\rho_2/\gamma_2 = 4 \times 10^{-4}$ ,  $\epsilon_1^2 = 2$ ,  $\epsilon_2^2 = 208$ . We observe that the model reproduces the qualitative features of the data, as seen in Fig. 5, including the observed improved performance at lower PA<sub>1</sub> gain levels.

---